Applied Surface Science 428 (2018) 877–884

Contents lists available at ScienceDirect

Applied Surface Science

journal homepage: www.elsevier.com/locate/apsusc

Full length article

Gaseous material capacity of open plasma jet in plasma spray-physical vapor deposition process

Mei-Jun Liu[a], Meng Zhang[a], Qiang Zhang[a,b], Guan-Jun Yang[a,*], Cheng-Xin Li[a], Chang-Jiu Li[a]

[a] State Key Laboratory for Mechanical Behavior of Materials, School of Materials Science and Engineering, Xi'an Jiaotong University, Xi'an, Shaanxi 710049, PR China
[b] AVIC Beijing Institute of Aeronautical Materials, Beijing, 100094, PR China

ARTICLE INFO

Article history:
Received 3 July 2017
Received in revised form
15 September 2017
Accepted 25 September 2017
Available online 28 September 2017

Keywords:
Gaseous material capacity
Vapor pressure
Local thermal equilibrium
PS-PVD

ABSTRACT

Plasma spray-physical vapor deposition (PS-PVD) process, emerging as a highly efficient hybrid approach, is based on two powerful technologies of both plasma spray and physical vapor deposition. The maximum production rate is affected by the material feed rate apparently, but it is determined by the material vapor capacity of transporting plasma actually and essentially. In order to realize high production rate, the gaseous material capacity of plasma jet must be fundamentally understood. In this study, the thermal characteristics of plasma were measured by optical emission spectrometry. The results show that the open plasma jet is in the local thermal equilibrium due to a typical electron number density from 2.1×10^{15} to 3.1×10^{15} cm^{-3}. In this condition, the temperature of gaseous zirconia can be equal to the plasma temperature. A model was developed to obtain the vapor pressure of gaseous ZrO_2 molecules as a two dimensional map of jet axis and radial position corresponding to different average plasma temperatures. The overall gaseous material capacity of open plasma jet, take zirconia for example, was further established. This approach on evaluating material capacity in plasma jet would shed light on the process optimization towards both depositing columnar coating and a high production rate of PS-PVD.

1. Introduction

Plasma spray-physical vapor deposition (PS-PVD) was emerged based on two powerful technologies of both plasma spray (PS) and physical vapor deposition (PVD). Owing to the high plasma energy (~120 kW) and the low chamber pressure (50–200 Pa), the feedstock powders can be melted even be vaporized in PS-PVD process [1,2]. Therefore, the coatings with different microstructure, such as lamellar coating, columnar coating and mixed coating, were produced by PS-PVD through adjusting the processing parameters (e.g. the feed rate) [3]. Among the available coatings, much attention has been paid to columnar coating deposited by vaporized coating material due to the excellent thermal shock resistance [4,5]. One of the necessary conditions for depositing the columnar coating is a higher vaporized coating material content in the open plasma jet. PS-PVD is expected to possess a higher production rate than conventional EB-PVD, because the vaporized coating material is transported in a hot and supersonic gas stream [2]. The maximum production rate is affected by many factors, such as material feed rate, but it is actually determined by the vapor capacity of transporting plasma. As a result, the gaseous material capacity of plasma jet in PS-PVD has to be fundamentally understood towards the high production rate.

To realize a higher production rate, the effective evaporation of feedstock powder in plasma jet is a fundamental issue, which is affected by two factors of particle size and powder feed rate. Recently, much attention has been paid to improve the evaporation of feedstock powders in the PS-PVD process [6]. It is reported that a high evaporation degree in the PS-PVD process can be obtained by adjusting process conditions like finer feedstock powders [7–9], suitable feed rate [7,10], and so on [11,12]. Agglomerated powder (7 wt.% yttria partially stabilized zirconia powder, Metco 6700, Sulzer-metco, Swizerland) with particle size ranging from 5 to 25 μm is typically used in PS-PVD [7,9,13]. The primary size of Metco 6700 powders is ranged from 70 to 130 nm [7,13]. In the PS-PVD process, the Metco 6700 powders were disintegrated well into small primary particles due to the weak agglomeration of primary particles [7,9,13]. As reported, a representative feedstock particle with diameter of 0.92 μm can be completely evaporated in the plasma torch nozzle where the heat flux is higher than 10^8

* Corresponding author.
E-mail address: ygj@mail.xjtu.edu.cn (G.-J. Yang).

https://doi.org/10.1016/j.apsusc.2017.09.218
0169-4332/

$W \cdot m^{-2}$ with Ar/He as the plasma gas [14]. Therefore, a great deal of these fine primary particles can be evaporated in the plasma torch nozzle due to large surface area of these particles exposed to high temperature plasma.

The evaporation degree of feedstock is not only affected by the particle size, but also affected by the powder feed rate. The heat value required to heat the ZrO_2 from solid state to complete evaporation is about 1058.5 $kJ \cdot mol^{-1}$. If the powder feed rate is 20 $g \cdot min^{-1}$, the energy required for total evaporation of ZrO_2 is 172.1 $kJ \cdot min^{-1}$. For a plasma torch with a power of 60 kW, the provided energy is 3600 $kJ \cdot min^{-1}$. Therefore, the heat energy provided by the plasma torch is sufficient to vaporize the ZrO_2 completely. However, the study found that the use of higher powder feed rate results in vaporizing more feedstock until a certain level (20 $g \cdot min^{-1}$) is reached, and the amount of vapor decreases with the further increase of powder feed rate [10]. Therefore, the variation of powder feed rate influences the evaporation degree of feedstock. In other words, the powder cannot be vaporized completely when the feed rate reaches a certain level. This limits the powder feed rate, and thereby a high production rate cannot realized.

The vaporized coating material and the plasma gas ejected from the plasma torch nozzle and formed an open plasma jet. The open plasma jet of PS-PVD can expand to a length of more than 2 m and 200–400 mm in diameter due to the low chamber pressure about 50 ~ 200 Pa [15]. The characteristics of open plasma jet are significantly different under such low pressure (about 50 ~ 200 Pa) [16,17]. Recently, OES is used to study the electron number density and the plasma temperature [17,18]. In addition, the optical emission of vaporized coating material is also studied by the OES [19]. However, there are different characteristics at different positions of open plasma jet, while the vaporized coating material transported in the plasma jet. Therefore, the states of vaporized coating material and the gaseous material capacity of open plasma jet will be affected by the characteristics of open plasma jet.

In this work, a methodology to obtain the powder feed rate by evaluating gaseous material capacity in open plasma jet was developed based on the optical emission spectrometry measurement. Firstly, the OES was used to examine the distribution of the electron number density and plasma temperature in different positions of open plasma jet. Then, take ZrO_2 for example, the local vapor pressure of gaseous ZrO_2 molecules is calculated by the distribution of average plasma temperature. Finally, the gaseous material capacity at different axial positions of open plasma jet was established. This study on evaluating material capacity of open plasma jet would shed light on the process optimization towards both depositing columnar coating with gaseous phase and a high production rate of PS-PVD.

2. Evaluation method and experimental procedure

As mentioned in "Introduction", the necessary condition for the deposition of columnar coating is a higher vapor content of feedstock powders in the open plasma jet [2]. The vaporized coating material has a long transport distance in the open plasma jet before reaching the substrate and forming the coating. Therefore, the states of vaporized coating material will be affected by the characteristics of open plasma jet. Moreover, the vaporized coating material tends to be condensed inside the open plasma jet as the characteristics of open plasma jet changes. The necessary condition for the condensation of vaporized coating material is the partial pressure higher than the vapor pressure [20]. Thus, it is important to study the vapor pressure of coating material to estimate whether the vaporized coating material are condensed.

For each substance, the vapor pressure is the partial pressure under saturated conditions when gaseous and liquid phase are in equilibrium, and it is the function of temperature [20]. The temperature of vaporized coating material is equal to the plasma temperature based on the theory of local thermal equilibrium (LTE) because the temperature of all species can be regarded as same under LTE condition [21,22]. Hence, the vapor pressure of feedstock powders can be studied by the plasma temperature. Then the gaseous material capacity in a specific position can be calculated by the vapor pressure gained above.

2.1. Evaluation method

The schematic diagram of OES detection is shown in Fig. 1. As shown in Fig. 1(a), a Cartesian coordinate system is established to describe the open plasma jet. A lens is used to collect the lights emitted from the open plasma jet. The collected lights are transmitted through the optical fiber to the spectrometer, and the detecting signal is recorded by computer, as shown in Fig. 1(b). The detecting region of OES is shown in Fig. 1(c). It is regards as a cylinder of which the bottom diameter and high is 15 mm and 300 mm, respectively. However, the diameter of plasma jet is about 170 mm in this work. Thus, the detecting region of OES in plasma jet is φ15 mm × 170 mm. The radial detecting position of open plasma jet is 0 mm, 15 mm, 30 mm and 45 mm, respectively.

2.1.1. Examination of electron number density

Plasma characteristics are investigated by OES. Even plasma not in LTE state, the electron number density is calculated by using the Stark broadening method [17,18]. In this work, the H_β line of the Balmer series of hydrogen at 486.13 nm is used to calculate the electron number density [18,23,24]:

$$\log n_e = 1.452 \log \Delta\lambda_{1/2} + 16.017 \quad (1)$$

where n_e is the electron number density (cm^{-3}) and $\Delta\lambda_{1/2}$ is the full-width at half-maximum (nm).

There are some effects which give rise to Gaussian line shapes contributing to line broadening such as the instrument broadening and the Doppler broadening. These effects tend to be independent from those producing Lorentzian broadening profiles. Since the Lorentzian half-width is used to calculate the electron number density and only Stark broadening causes a significant Lorentz contribution [17]. In order to separate the Gauss and Lorentz contributions, a Voigt function, which is the convolution of a Lorentz and a Gauss function, is used to fit the spectral line [17,23].

2.1.2. Examination of plasma temperature

In the LTE state, the temperature of all species (such as atoms, ions, and electrons) can be regarded to be same and be equal to the plasma temperature, meanwhile, the calculation of plasma temperature can be carried out by using the method of double spectral lines [25,26]:

$$\frac{I_{ji}}{I_{kl}} = \frac{\lambda_{kl} A_{ji} g_j}{\lambda_{ji} A_{kl} g_k} \exp\left(\frac{E_k - E_j}{k_B T}\right) \quad (2)$$

where I_{ji} (a.u.) is the spectral intensity generated by the transition from energy level j to i, I_{kl} (a.u.) is the spectral intensity generated by the transition from energy level k to l, λ_{ji} (nm) is the wavelength in the spectrum generated by the transition from energy level j to i, λ_{kl} (nm) is the wavelength in the spectrum generated by the transition from energy level k to l, A_{ji} (s^{-1}) is the Einstein spontaneous transition probability from energy level j to i, A_{kl} (s^{-1}) is the Einstein spontaneous transition probability from energy level k to l, g_j is the statistical weight of energy level j, g_k is the statistical weight of energy level k, E_j (eV) is the excitation energy of energy level j, E_k (eV) is the excitation energy of energy level k, and k_B is

the Boltzmann constant. The light intensity (I_{ji} and I_{kl}) can be measured experimentally. The other parameters can be obtained from the National Institute of Standards and Technology (NIST) database.

Generally, Abel inversion is used to reconstruct the spatial characteristics of the plasma jet [27,28]. He et al. were reconstructs the local emission intensity $\varepsilon(r)$ from the measured intensity $I(y)$, and calculated the local excitation temperature [29]. However, in this work, the feedstock powders were radially injected to the plasma torch, possibly resulting in a non-axisymmetric distribution of plasma temperature. Thus, the spectra were not Abel inverted. The calculated temperature depending on $I(y)$ is called the average plasma temperature.

2.1.3. The vapor pressure of ZrO_2

The vapor pressure of ZrO_2 at different positions of open plasma jet is calculated by the plasma temperature. The following assumptions are employed to the calculation of this work:

(1) The pressure of open plasma jet is assumed to be equal to the chamber pressure.

(2) The ideal gas law is applicable.

When two phases α and β are in equilibrium, their chemical potentials ($\mu(p, T)$) must be equal. Therefore,

$$\mu_\alpha(p, T) = \mu_\beta(p, T) \tag{3}$$

where p and T is the pressure and the temperature in equilibrium, respectively.

By solving this equation for p in terms of T, we get the Clapeyron equation for the phase boundary.

$$\frac{dp}{dT} = \frac{\Delta_\alpha^\beta H_m}{T\Delta_\alpha^\beta V_m} \tag{4}$$

where p is the two phase equilibrium pressure (Pa), T is the two phase equilibrium temperature (K), $\Delta_\alpha^\beta H_m$ is the molar enthalpy of phase transition (J·mol^{-1}), $\Delta_\alpha^\beta V_m$ is the molar volume of phase transition (m^3).

In liquid-vapor equilibrium, $\Delta_\alpha^\beta V_m$ can be written as $\Delta_\alpha^\beta V_m \approx V_m(g)$ (where $V_m(g)$ is the molar volume of perfect gas) because the molar volume of gas is much greater than the molar volume of liquid. According to the ideal gas law, $V_m(g) = RT/p$. Moreover, it can be considered that $\Delta_\alpha^\beta H_m$ does not change when the change of temperature is small. Therefore, the exact Clapeyron is transformed into:

$$\ln\frac{p_2}{p_1} = -\frac{\Delta_l^g H_m}{R}\left(\frac{1}{T_2} - \frac{1}{T_1}\right) \tag{5}$$

where both T_1 and T_2 are the two phase equilibrium temperature (K), both p_1 and p_2 are the vapor pressure (Pa), $\Delta_l^g H_m$ is the molar enthalpy of vaporization (J·mol^{-1}), R is the gas constant, R = 8.31 Pa·m^3·mol^{-1}·K^{-1}. According to Eq. (5), we can calculate the vapor pressure at different temperatures.

2.1.4. Calculation of the gaseous material capacity

The amount of gaseous ZrO_2 molecules under the vapor pressure is the maximum number of gaseous ZrO_2 molecules allowed pass through the OES detection region in the time of 80 ms. At the OES detection region, the maximum amount of gaseous ZrO_2 molecules is calculated by the local temperature and pressure when the gaseous ZrO_2 molecules conforms to the ideal gas law.

$$pV = nRT = \frac{N_{\max,z,y}}{N_A}RT \tag{6}$$

where T is the plasma temperature, p is the vapor pressure of ZrO_2, V is the volume of OES detecting region (V = 3.00 × 10^{-5} m^3, Fig. 1(c)), n is the amount of substance of zirconia vapor (mol), $N_{max,z,y}$ is the maximum amount of gaseous ZrO_2 molecules in the OES detecting region, z is the position of Z axial direction (z = 90, 180, 270, 360, 450 mm), y is the position of Y axial direction (y = 0, 15, 30, 45 mm), N_A is the Avogadro's constant (6.02 × 10^{23} mol^{-1}).

According to the distribution of gaseous ZrO_2 molecules number along the Z and Y axial direction and the dissociation fraction of ZrO_2, the total amount of gaseous zirconia ($N_{max,z}$, including ZrO_2, ZrO and Zr) in different positions of Z axis can be calculated.

$$N_{\max,z} = \sum N_{zirconia,z,y} \tag{7}$$

where $N_{zirconia,z,y}$ is the maximum amount of gaseous zirconia in the OES detecting region.

The localized gaseous material capacity of open plasma jet corresponding to the different positions of Z axis can be calculated as follow.

$$m = \frac{N_{max,z}}{N_A} \times M_{ZrO_2} \times \frac{60}{t} \tag{8}$$

where m is the localized gaseous material capacity corresponding to a Z axial direction position (g·min^{-1}), M_{ZrO_2} is the relative molecular mass of ZrO_2, 123.22 g·mol^{-1}, t is the detection time of the OES, 80 ms.

2.2. Experimental procedure

2.2.1. Diagnosis of open plasma jet characteristics by OES

In this study, the characteristics of open plasma jet are detected by OES. The specific detection method is described as following. As shown in Fig. 1, in a Z axial position, the lights emitted from different radial positions are collected by a lens (FC-446-030, Andor Technology, UK), then are transported to the spectrometer (Acton SP2750, Princeton Instruments, USA) by an optical fiber. Finally, the detected spectral signal is reported by computer. For data acquisition, the lights emitted from the open plasma jet are diagnosed by a grating with 300 grooves/mm, the spectrometer resolution is 0.058 nm, and the exposure time is 80 ms. The spectral region from 300 to 1000 nm is selected. The calibration of the spectrometer is carried out with a standard mercury lamp before detection.

2.2.2. Processing parameters

A commercial plasma spray torch (F6, 80 kW class, GTV, Germany) mounted on a six-axis robot (Lab-modified IRB 1600, ABB, Sweden) is placed in a 10 m^3 vacuum chamber as spray system. The plasma spraying parameters used in this work are listed in Table 1.

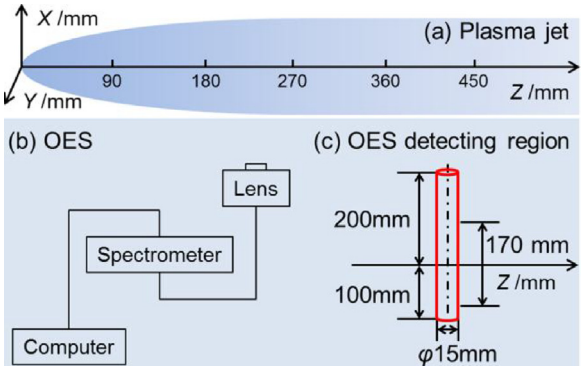

Fig. 1. Method used for detecting open plasma jet.

Table 1
Processing parameters.

Parameter	Unit	Value
Power	kW	60
Current	A	750
Chamber pressure	Pa	100
Ar flow	SLPM	60
H_2 flow	SLPM	12
Axial detection distance (Z axis)	mm	90/180/270/360/450
Radial detection distance (Y axis)	mm	0/15/30/45
Feedstock powder		Metco 6700 (Sulzer-metco)
Powder feed rate	g·min^{-1}	0.5

3. Results and discussions

3.1. Electron number density of open plasma jet

Fig. 2 shows the optical spectrum of open plasma jet examined by the OES. Atomic lines of hydrogen (H_α (656.279 nm) and H_β (486.15 nm)) are detected from the spectrum. As shown in Fig. 2(a) and (b), the intensity of spectral lines coming from position of Y = 0 mm is higher than that coming from Y = 30 mm due to a higher plasma density and temperature at the center of open plasma jet. In addition, the intensity of spectral lines at Z = 90 mm is higher than that at Z = 450 mm due to the expansion of open plasma jet leading to thinner plasma gas, lower plasma density and temperature. In addition, the intensity of the spectra was too low to calculate the electron number density accurately when Y > 45 mm. Therefore, the radial detecting distance of open plasma jet is ≤45 mm.

The distributions of electron number density along Z axis and Y axis are shown in Fig. 3. It can be seen that the electron number density decreased with the increase of Z axial distance due to the density of plasma gas decreased with the expansion of open plasma jet. In the Y axial direction, the electron number density decreased with the increase of Y axial distance because the open plasma jet has a lower intensity in the position far away from the center. The electron number density is ranged from 2.1×10^{15} to 3.1×10^{15} cm^{-3} in the whole region of open plasma jet.

3.2. Identification of local thermal equilibrium state

For detection of plasma temperature based on OES, the thermal equilibrium or local thermal equilibrium (LTE) condition is necessary. But there is insufficient time for PS-PVD process to achieve complete thermal equilibrium [21]. In fact, it is possible to estimate the plasma temperature as long as the LTE is satisfied. When the plasma satisfies the LTE, the processes in the plasma can be described by the same temperature except the radiation process [30], which implies that electron temperature T_e, heavy particles temperature T_h, ionization temperature T_{Saha} and excitation temperature T_{exc} are all equal [17].

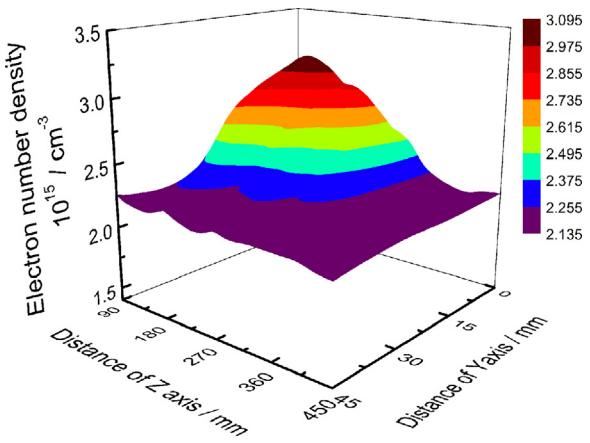

Fig. 3. Two dimensional map of electron number density of open plasma jet.

To establish the LTE in the plasma, it does require that collision processes to control transitions and reactions [30]. The collision processes plays a dominated role means there must be large electron number densities existing in the plasma [31,32]. Therefore, the electron number density is one of the key requirements for LTE, and it can be used to determine the plasma in LTE state. A necessary criterion for LTE is given by the following formula [18,33]:

$$n_e^* \geq 1.4 \times 10^{14} \times T_e \Delta E^3 \quad (9)$$

where n_e^* is the critical value of electron number density for LTE, T_e is in eV, ΔE is the energy difference between higher and lower energy levels (in eV).

Eq. (2) can be used to calculate the electron temperature even the open plasma jet is not in the LTE state [26]. The electron temperatures calculated by Eq. (2) at different positions of open plasma jet are shown in Fig. 4. The electron temperature is ranged from 3650 K to 4270 K. Through the conversion of Boltzmann constant, the electron temperature of open plasma jet is about 0.31 ~ 0.37 eV in this work.

The critical value of electron number density calculated by Eq. (9) is about $7.2 \times 10^{14} \sim 8.6 \times 10^{14}$ cm^{-3}. The calculated values of electron number density (10^{15} cm^{-3}) in part 3.1 are greater than this limit range. Therefore, the LTE approximation for this work is valid for estimation in subsequent analysis.

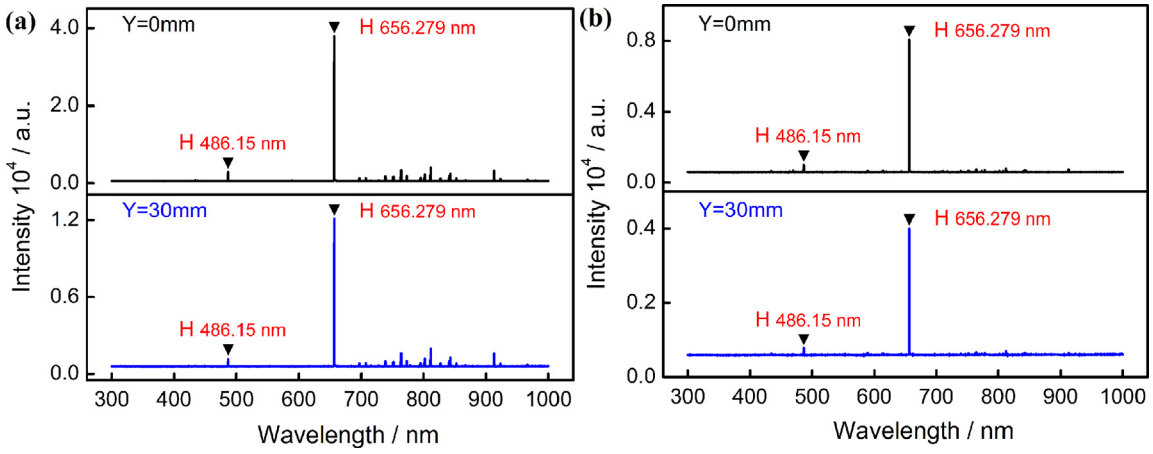

Fig. 2. Optical spectrum of the open plasma jet. (a) Z axis position is 90 mm, (b) Z axis position is 450 mm.

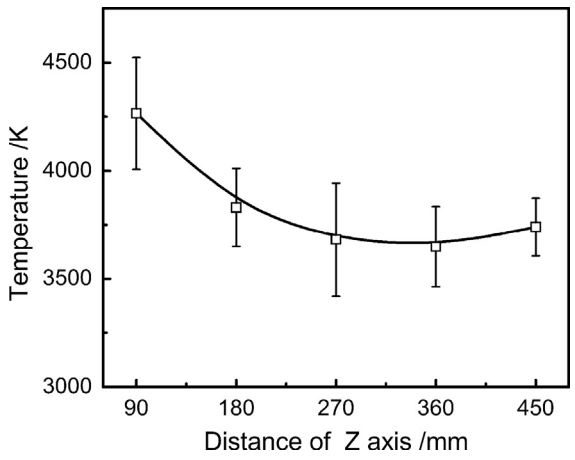

Fig. 4. The electron temperature of open plasma jet.

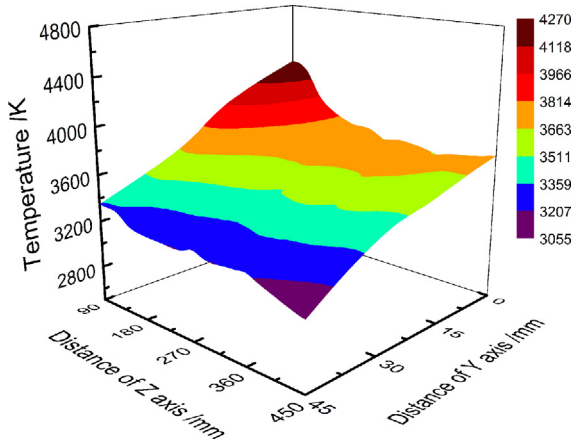

Fig. 5. Two dimensional map of plasma temperature of open plasma jet.

3.3. Local average temperature of open plasma jet

In the LTE condition, the local average plasma temperature is calculated by using the double spectral lines method in Eq. (2). As shown in Fig. 2, the light intensity of selected H_α and H_β signals are corresponding to I_{ji} and I_{kl}, respectively. The distribution of local average plasma temperature is shown in Fig. 5. It can be seen that the local average plasma temperature gradually reduced and then kept steady when the Z axial distance increased from 90 mm to 450 mm. It can also be seen that the change of the local average plasma temperature along Y axial direction is similar to that at Z axis. These are resulted from the expansion of the open plasma jet, and the local average plasma temperatures are ranged from 3055 K to 4270 K in the whole region of open plasma jet. In addition, from Figs. 2 and 3, the H_α line is found to be self-absorbing in the position of higher plasma density. Therefore, the determination results of plasma temperature will be affected by self-absorbing of H_α line. The intensity of H_α line decreases due to the self-absorbing causing the calculated temperature a little bit less than the actual temperature.

When the Y axial distance less than or equal to 30 mm, the local average plasma temperature is higher than 3247 K in the entire Z axis. The 3247 K is a specific temperature for ZrO_2, because the vapor pressure of ZrO_2 in this temperature is the chamber pressure (100 Pa) used in this study. There is a condensation trend for the gaseous ZrO_2 molecules when the temperature is lower than 3247 K. On the contrary, when the temperature is higher than 3247 K, the condensation trend will occur only when the partial pressure of gaseous ZrO_2 molecules higher than the vapor pressure.

3.4. The vapor pressure of gaseous ZrO_2

The temperature of gaseous ZrO_2 molecules is equal to the plasma temperature due to the same temperature of all species in the open plasma jet during in the LTE condition. Therefore, the vapor pressure of ZrO_2 molecules in different positions of open plasma jet is calculated by the local average plasma temperature. The distribution of vapor pressures of ZrO_2 molecules along the Z axis and Y axis is shown in Fig. 6. The vapor pressures of ZrO_2 molecules decreased with the increase of Z axial and Y axial distance. Furthermore, the higher the plasma temperature, the higher the vapor pressure, for the vapor pressure is the function of temperature. The green curve in Fig. 6(a) represents the chamber pressure (100 Pa). Fig. 6(b) shows clearly that the vapor pressure of ZrO_2 molecules is greater than 100 Pa during the distance of Y axis less than 45 mm.

The 100 Pa is a key pressure to determine whether the gaseous ZrO_2 molecules will be condensed. As observed in Fig. 6, the vapor pressure of ZrO_2 molecules is higher than 100 Pa in the entire Z axis when Y axial distance is less than 45 mm. The gaseous ZrO_2 molecules will not be condensed in this region due to the partial pressure of gaseous ZrO_2 molecules lower than 100 Pa. On the contrary, the condensation of ZrO_2 molecules can occur in distance greater than 30 mm. Based on the thermodynamic conditions of nucleation, when the saturated vapor pressure is lower than

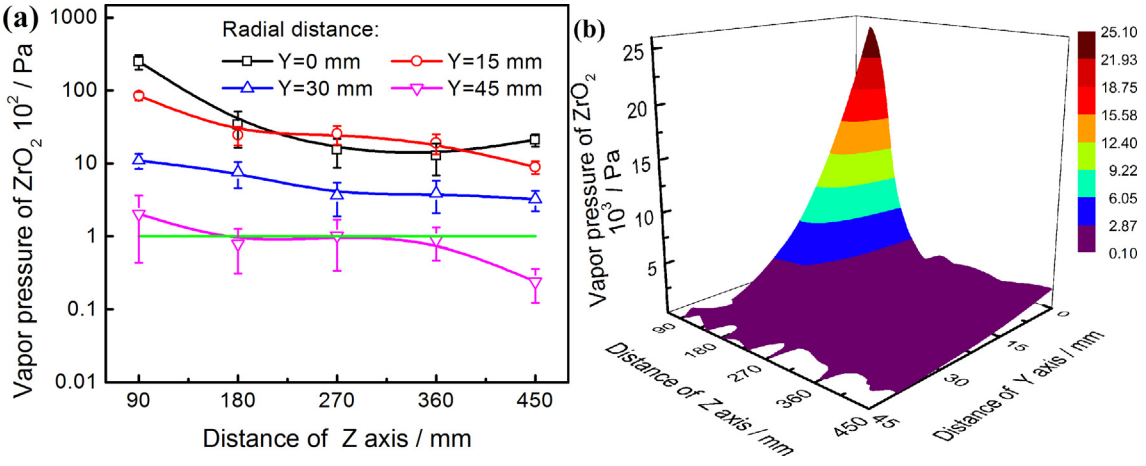

Fig. 6. Distribution of vapor pressure of ZrO_2.

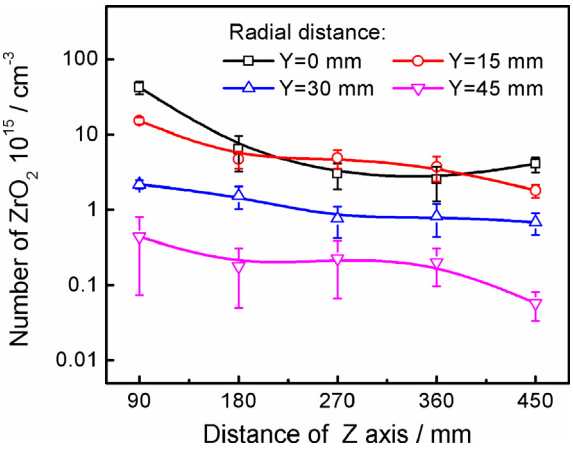

Fig. 7. The distribution of gaseous ZrO_2 molecules number along Z axis.

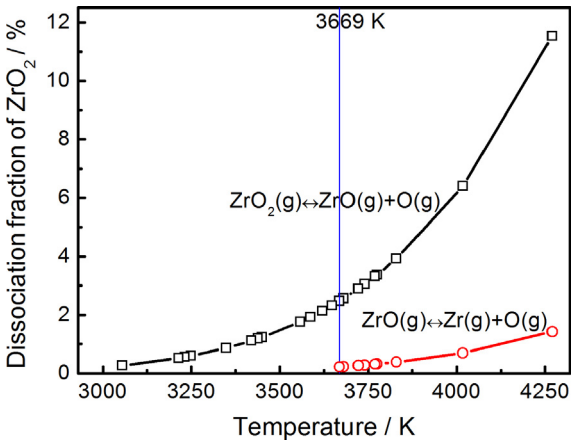

Fig. 8. The dissociation fraction of ZrO_2 and ZrO in different temperature at the chamber pressure (100 Pa).

environmental pressure, if the partial pressure of gaseous ZrO_2 molecules in the open plasma jet greater than the saturated vapor pressure, the condensation would happen.

3.5. Gaseous material capacity of open plasma jet

The lights emitted from the plasma gas are collected by OES in the detection region in 80 ms. In the same detection region, the plasma gas properties are similar in different time due to the constant of spray parameters. Therefore, the capacity of gaseous ZrO_2 molecules calculated by the vapor pressure is the maximum number allowed to pass through the detection region in 80 ms.

The distribution of gaseous ZrO_2 molecules number is shown in Fig. 7. The amount of gaseous ZrO_2 molecules varies with the different positions due to the diverse local vapor pressure of open plasma jet. In the whole range of open plasma jet, the gaseous ZrO_2 molecules number is ranged from 5.7×10^{14} cm^{-3} to 4.3×10^{17} cm^{-3}. It is decreased along the Z and Y axial direction as the plasma jet expanded. The closer to the nozzle, the more gaseous ZrO_2 molecules are accommodated.

The distribution of gaseous ZrO_2 molecules number along Z axis is obtained in the above section. However, in the PS-PVD process, the gaseous ZrO_2 molecules will dissociate to ZrO, Zr and O. The total pressure of the gaseous zirconia (including ZrO_2, ZrO, Zr and O) in plasma jet will be estimated from Dalton's law:

$$P = \left(n_{ZrO_2} + n_{ZrO} + n_{Zr} + n_O\right) k_B T \quad (10)$$

where P is the total pressure of ZrO_2, ZrO, Zr and O, k_B is Boltzmann constant, T is the temperature, n_{ZrO_2}, n_{ZrO}, n_{Zr} and n_O is the mole fractions of ZrO_2, ZrO, Zr and O, respectively.

According to Eq. (10), the total pressure must be considered during calculate the total mole fractions of the gaseous zirconia. There are two equilibrium processes when the gaseous ZrO_2 molecules are dissociated to ZrO, Zr and O:

$$ZrO_2(g) \leftrightarrow ZrO(g) + O(g)(6.5 \pm 0.2\,eV) \quad (11)$$

$$ZrO(g) \leftrightarrow Zr(g) + O(g)(7.89 \pm 0.1\,eV) \quad (12)$$

Therefore, as long as the dissociation fractions of ZrO_2 and ZrO at different temperatures are calculated, the total mole fractions of the gaseous zirconia can be obtained even the total pressure unknown.

The NASA Chemical Equilibrium with Applications (CEA) software was used to check the mole fraction of the gaseous zirconia by assigning discrete temperatures and the chamber pressure (100 Pa). The dissociation fractions of ZrO_2 and ZrO at different temperatures were further calculated based on the checked results, and the calculation results are shown in Fig. 8. The dissociation process of ZrO_2 occurs in the entire range of investigated temperature. The dissociation fraction of ZrO_2 is increased with the increase in temperature. At 4270 K, the maximum dissociation ratio of ZrO_2 is 11.5%. The dissociation process of ZrO occurs only when the temperature is higher than 3669 K in this work. Meanwhile, the dissociation fraction of ZrO is much lower than the ZrO_2 because the dissociation of ZrO needs more energy.

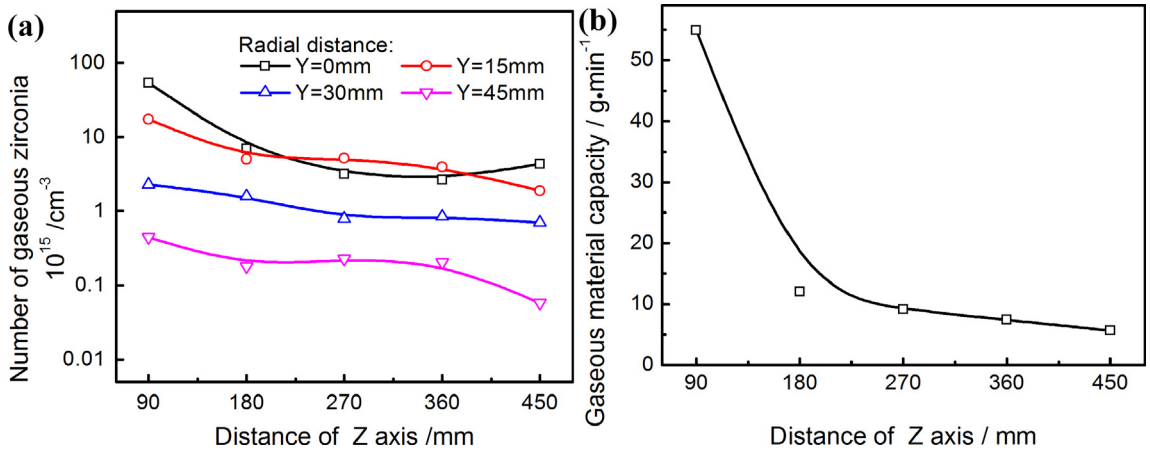

Fig. 9. The distribution of total gaseous zirconia number and gaseous material capacity along Z axis. (a) The distribution of total gaseous zirconia number along Z axis, (b) the gaseous material capacity restricted by vapor pressure of the gaseous zirconia along Z axis.

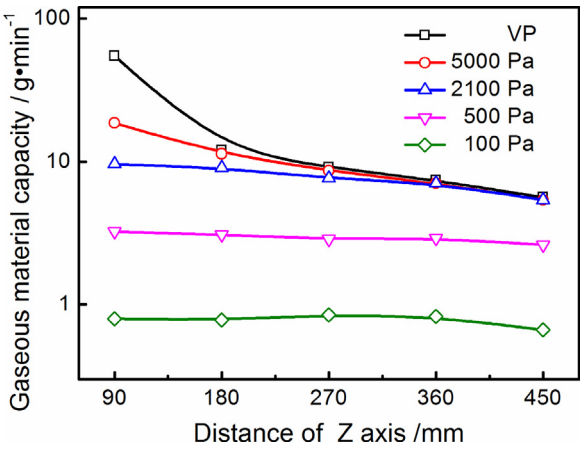

Fig. 10. The gaseous material capacity of open plasma jet under different chamber pressure. Herein, VP means gaseous material capacity restricted by vapor pressure of the gaseous zirconia.

The distribution of the total gaseous zirconia number can simply calculated by the data of Figs. 7 and 8, and the results are shown in Fig. 9(a). Since the dissociation ratio of gaseous ZrO_2 molecules is a function of temperature, the distribution of the total gaseous zirconia number is the same as the gaseous ZrO_2 molecules. The total gaseous zirconia number is ranged from 5.8×10^{14} cm^{-3} to 5.4×10^{17} cm^{-3}.

The localized gaseous material capacity of open plasma jet is shown in Fig. 9(b). It is ranged from 54.9 g·min^{-1} to 5.6 g·min^{-1} in the whole region of open plasma jet. The total gaseous material capacity of open plasma jet is limited by the local vapor pressure of the gaseous zirconia and should be less than 5.6 g·min^{-1}.

3.6. *The gaseous material capacity restricted by both chamber pressure and vapor pressure*

According to above results, the gaseous material capacity of open plasma jet can reach 5.6 g·min^{-1}. However, the powder feed rate can only be kept around 0.5 g·min^{-1} in this work because the gaseous material capacity is restricted by both the partial pressure and vapor pressure of gaseous zirconia in the open plasma jet. According to the Dalton's law, the chamber pressure (assumed equal to open plasma jet pressure, part 2.1.4) is equal to the sum of the partial pressure of gaseous zirconia and the partial pressure of plasma gas. Hence, the partial pressure of gaseous zirconia is lower than chamber pressure. In fact, the higher the chamber pressure is, the higher the partial pressure of gaseous zirconia is allowed. Therefore, it is possible to qualitatively examine the gaseous material capacity with Z axial position using chamber pressure instead of partial pressure of gaseous zirconia. When the chamber pressure is less than the vapor pressure of gaseous zirconia, the gaseous material capacity is calculated by using chamber pressure. On the contrary, the capacity is calculated by using the vapor pressure of zirconia.

Fig. 10 shows the gaseous material capacity of open plasma jet under different chamber pressure. The black curve in Fig. 10 represents the gaseous material capacity limited by the vapor pressure of gaseous zirconia (as shown in Fig. 9(b)). The gaseous material capacity would be higher with the increase of chamber pressure. The chamber pressure about 2100 Pa is approach to the maximum vapor pressure of zirconia at 450 mm position. In this condition, the gaseous material capacity at position of 450 mm is restricted by the vapor pressure of gaseous zirconia. Furthermore, when the chamber pressure is above 2100 Pa, the gaseous material capacity of the jet at position of 450 mm will be limited by the vapor pressure of gaseous zirconia and maintain at 5.6 g·min^{-1}, such as red curve with the chamber pressure at 5000 Pa, shown in Fig. 10. This means that, due to the limitation of vapor pressure of gaseous zirconia, the gas phase capacity of the jet cannot be improved even the chamber pressure is increased.

Actually, the partial pressure of gaseous zirconia is lower than the chamber pressure, and it can be increased with the chamber pressure. Therefore, the actual gaseous material capacity is smaller than that calculated by the chamber pressure. Take 100 Pa for example, the gaseous material capacity is limited to 0.66 ~ 0.85 g·min^{-1} as shown in Fig. 10. As mentioned in the above, the partial pressure of gaseous zirconia in the open plasma jet is less than 100 Pa. Therefore, the real gaseous material capacity should be below 0.66 g·min^{-1}, that is why the powder feed rate under this experimental condition is only 0.5 g·min^{-1}.

4. Conclusions

In PS-PVD process, the gaseous material capacity of open plasma jet is the necessary condition for both depositing columnar coating and a higher production rate. Actually, the gaseous material capacity is affected by the characteristics of open plasma jet. In this work, the characteristics of plasma are measured by OES. The results show that the open plasma jet is being in the local thermal equilibrium. A model is developed to obtain the vapor pressure of ZrO_2 as a two dimensional map of jet axis position and jet radial position corresponding to different plasma temperatures. The distribution of the maximum gaseous ZrO_2 molecule number of open plasma jet is obtained. Meanwhile, the dissociation fractions of ZrO_2 and ZrO at different temperatures are calculated based on the checked results of NASA CEA software. The distribution of the total gaseous zirconia number is calculated to obtain the localized gaseous material capacity of open plasma jet. The actual gaseous material capacity is restricted by both the partial pressure and vapor pressure of gaseous zirconia in open plasma jet, and more gaseous material capacity is held during the higher chamber pressure and plasma temperature. This approach on evaluating material capacity in open plasma jet would shed light on the adjustment and optimization of PS-PVD spraying process.

Acknowledgments

This project was supported by the National Basic Research Program of China (No. 2013CB035701), the Fundamental Research Funds for the Central Universities, and the National Program for Support of Top-notch Young Professionals.

References

[1] K. von Niessen, M. Gindrat, A. Refke, Vapor phase deposition using plasma spray-PVD (TM), J. Therm. Spray Technol. 19 (2010) 502–509.
[2] K. von Niessen, M. Gindrat, Plasma spray-PVD: a new thermal spray process to deposit out of the vapor phase, J. Therm. Spray Technol. 20 (2011) 736–743.
[3] B.J. Harder, D. Zhu, Plasma spray-physical vapor deposition (PS-PVD) of ceramics for protective coatings, in: D. Zhu, H.T. Lin, Y. Zhou, S. Widjaja, D. Singh (Eds.), Advanced Ceramic Coatings and Materials for Extreme Environments, 2011, pp. 73–84.
[4] M. Goral, S. Kotowski, A. Nowotnik, M. Pytel, M. Drajewicz, J. Sieniawski, PS-PVD deposition of thermal barrier coatings, Surf. Coat. Technol. 237 (2013) 51–55.
[5] S. Rezanka, G. Mauer, R. Vaßen, Improved thermal cycling durability of thermal barrier coatings manufactured by PS-PVD, J. Therm. Spray Technol. 23 (2014) 182–189.
[6] G. Mauer, M.O. Jarligo, S. Rezanka, A. Hospach, R. Vassen, Novel opportunities for thermal spray by PS-PVD, Surf. Coat. Technol. 268 (2015) 52–57.
[7] A. Hospach, G. Mauer, R. Vaßen, D. Stoever, Characteristics of ceramic coatings made by thin film low pressure plasma spraying (LPPS-TF), J. Therm. Spray Technol. 21 (2012) 435–440.

[8] B. Vautherin, M.P. Planche, R. Bolot, A. Quet, L. Bianchi, G. Montavon, Vapors and droplets mixture deposition of metallic coatings by very low pressure plasma spraying, J. Therm. Spray Technol. 23 (2014) 596–608.
[9] X.F. Zhang, K.S. Zhou, C.M. Deng, M. Liu, Z.Q. Deng, C.G. Deng, J.B. Song, Gas-deposition mechanisms of 7YSZ coating based on plasma spray-physical vapor deposition, J. Eur. Ceram. Soc. 36 (2016) 697–703.
[10] G. Mauer, A. Hospach, R. Vaßen, Process development and coating characteristics of plasma spray-PVD, Surf. Coat. Technol. 220 (2013) 219–224.
[11] M. Gindrat, H.-M. Höhle, K. Niessen, P. Guittienne, D. Grange, C. Hollenstein, Plasma spray-CVD: a new thermal spray process to produce thin films from liquid or gaseous precursors, J. Therm. Spray Technol. 20 (2011) 882–887.
[12] Q.Y. Chen, C.X. Li, J.Z. Zhao, G.J. Yang, C.J. Li, Microstructure of YSZ coatings deposited by PS-PVD using 45 kW shrouded plasma torch, Mater. Manuf. Process. 31 (2016) 1183–1191.
[13] G. Mauer, A. Hospach, N. Zotov, R. Vaßen, Process conditions and microstructures of ceramic coatings by gas phase deposition based on plasma spraying, J. Therm. Spray Technol. 22 (2013) 83–89.
[14] G. Mauer, Plasma Characteristics and plasma-feedstock interaction under PS-PVD process conditions, Plasma Chem. Plasma Process. 34 (2014) 1171–1186.
[15] C. Li, H. Guo, L. Gao, L. Wei, S. Gong, H. Xu, Microstructures of yttria-stabilized zirconia coatings by plasma spray-physical vapor deposition, J. Therm. Spray Technol. 24 (2015) 534–541.
[16] E. Muehlberger, Method of Forming Uniform Thin Coatings on Large Substrates, in, US, 1998.
[17] G. Mauer, R. Vaßen, Plasma Spray-PVD: Plasma characteristics and impact on coating properties, in: A. Gleizes, E. Ghedini, M. Gherardi, P. Sanibondi, G. Dilecce (Eds.), 12th High-Tech Plasma Processes Conference (2012).
[18] N. Zhang, F. Sun, L. Zhu, M.P. Planche, H. Liao, C. Dong, C. Coddet, Electron temperature and density of the plasma measured by optical emission spectroscopy in VLPPS conditions, J. Therm. Spray Technol. 20 (2011) 1321–1327.
[19] Y. Gao, D. Yang, C. Sun, Z. Chen, Deposition of YSZ coatings in a chamber at pressures below 100 Pa using low-power plasma spraying with an internal injection powder feeding, J. Therm. Spray Technol. 22 (2013) 1253–1258.
[20] W.P. Atkins, Atkins' Physical Chemistry, Higher Education Press, 2006.
[21] Q.Y. Chen, X.Z. Peng, G.J. Yang, C.X. Li, C.J. Li, Characterization of plasma jet in plasma spray-physical vapor deposition of YSZ using a <80 kW shrouded torch based on optical emission spectroscopy, J. Therm. Spray Technol. 24 (2015) 1–8.
[22] L. Torrisi, F. Caridi, D. Margarone, A. Borrielli, Characterization of laser-generated silicon plasma, Appl. Surf. Sci. 254 (2008) 2090–2095.
[23] A.A. Ovsyannikov, M.F. Zhukov, Plasma Diagnostics, Cambridge International Science, Cambridge, 1995.
[24] N.K. Joshi, S.N. Sahasrabudhe, K.P. Sreekumar, N. Venkatramani, Axial variation of electron number density in thermal plasma spray jets, Eur. Phys. J. D 26 (2003) 215–219.
[25] J.H. Cui, Z.F. Xu, J.L. Zhang, Online diagnosis of electron excitation temperature in $CH_4 + H_2$ discharge plasma at atmospheric pressure by optical emission spectra, Sci. China Phys. Mech. Astron. 51 (2008) 1892–1896.
[26] N. Zhang, F. Sun, L. Zhu, C. Verdy, M.P. Planche, Characteristics of Cu film deposited using VLPPS, J. Therm. Spray Technol. 20 (2011) 351–357.
[27] L.M. Smith, D.R. Keefer, S.I. Sudharsanan, Abel inversion using transform techniques, J. Quant. Spectrosc. Radial. Transfer 39 (1986) 367–373.
[28] M. Kalal, K.A. Nugent, Abel inversion using fast Fourier transforms, Appl. Opt. 27 (1988) 1956–1959.
[29] W. He, G. Mauer, R. Vaßen, Excitation temperature and constituent concentration profiles of the plasma jet under plasma spray-pvd conditions, Plasma Chem. Plasma Process. 37 (2017) 1293–1311.
[30] M.I. Boulos, P. Fauchais, E. Pfender, Thermal Plasmas: Fundamentals and Applications, vol. 1, Plenum Press, 1994.
[31] S.S. Harilal, C.V. Bindhu, R.C. Issac, V.P.N. Nampoori, C.P.G. Vallabhan, Electron density and temperature measurements in a laser produced carbon plasma, J. Appl. Phys. 82 (1997) 2140–2146.
[32] N. Singh, M. Razafinimanana, A. Gleizes, The effect of pressure on a plasma plume: temperature and electron density measurements, J. Phys. D: Appl. Phys. 31 (1998) 2921–2928.
[33] H. Griem, Plasma Spectroscopy, McGraw-Hill Book Company, New York, 1964.